Supporting Information

Katz et al. 10.1073/pnas.1314485111

SI Materials and Methods

Fly Stocks. Flies used in this study were *yw*, w^{1118}, *en*-Gal4, *actin*-Gal4, *btl*-Gal4, *nub*-Gal4, *pumpless*-Gal4 (*ppl*-Gal4), *ms1096*-Gal4, UAS-p35, UAS-GFP, $thor^2$ (1), and *wRNAi* from the Bloomington *Drosophila* stock center (http://flystocks.bio.indiana.edu); *sud1* RNAi (#3402), UAS-DicerII, and *perk* RNAi (#110278) from the Vienna Drosophila RNAi Center (VDRC, http://stockcenter.vdrc.at/control/main); *btl*-Gal4 (2); and *ldh*-LacZ (3). UAS-Xbp1-GPF was a gift from Hermann Steller (The Rockefeller University, New York) (4). Helmut Kramer (University of Texas Southwestern Medical Center, Dallas) kindly provided the UAS-LAMP1-GFP line (5). UAS-ATG8-GFP was kindly provided by Thomas Neufeld (University of Minnesota, Minneapolis) (6). $rheb^{P\Delta1}$, $rheb^{P\Delta2}$ (7), TSC^{Q87X} (8), TOR^{2L1} (9), and $S6K^{L1}$ (10) were kindly provided by Sean Oldham (Sanford-Burnham Medical Research Institute, La Jolla, CA). In all experiments throughout this study, larvae were synchronized 24 h after egg deposition and grown at a controlled density (50 larvae per vial) in standard culture media at 25 °C or 29 °C depending on the experiment.

Cloning and Transgenic Lines Generation. Transgenic lines bearing the UAS-hOGFOD, UAS-wSud1, and bicistronic luciferase reporter were generated by phiC31-mediated site-directed integration on the 86F platform. The UAS-GFP-Sud1 was generated using the P element–mediated transformation method (11).

For the generation of the pUASt-wSud1 construct, the ORF of wSudestada was amplified by PCR from *Drosophila willistoni* females (EHIME University) cDNA using the following primers: 5′-GGAAGATCTATGGACACGGCCGAATCCAC-3′ and 5′-AAGGAAAAAAGCGGCCGCTTACTCCTTGTAACTACATGACATC-3′. The amplified fragment was subcloned into the pCR 2.1 TOPO vector (Invitrogen #45-0641) and was then cloned into the pUASt attb vector using KpnI and XhoI restriction sites. The ORF from hOGFOD was subcloned into the pUASt attb using the BamHI and XbaI restriction sites.

For the generation of the UAS-GFP-Sud1 construct, the Sud1 ORF was amplified by PCR from the first-instar larvae cDNA template using the following primers: 5′-CACCATGGAAACCTCGAGCT-3′ and 5′-CTACTCCTTGTAGCTGCACGAAAT-3′. The amplified fragment was subcloned using the pENTR/D-Topo clonig kit (Invitrogen #45-0218) and then cloned into the gateway pTGW expression plasmid.

N-terminally truncated human $RPS23_{44–143}$ was cloned into a bacterial expression vector providing an *N*-terminal GST-tag. Full-length *Drosophila melanogaster* Sudestada1 was cloned into the pET-28a vector with the *N*-terminal His_6-tag from CG44254 cDNA (isoform A) on the pUAS.g attb plasmid.

Real-Time PCR. Total RNA was isolated using the TRIzol reagent (Invitrogen). Genomic DNA was removed from RNA samples using the Ambion's DNA free kit. RNAs (1–1.5 μg) were reverse-transcribed using the superscript III First-strand synthesis system (Invitrogen) and oligo-dT as a primer. The resulting cDNA was used for real-time PCR (Stratagene MX300 sp), using Taq DNA polymerase (Invitrogen) and SYBRGreen and ROX (Invitogen) as fluorescent dyes. *Sud*- and *Bip*-specific primers were used. Samples were normalized using *tub* primers. Three independent biological samples were analyzed in each experiment. One representative set of results is shown for each experiment. Primer sequences were as follows: *Sud2* Fw, GCCAGTTGCTCATCGCCGAACT; *Sud2* Rv, GCGTGTGTGCTTCCTGGGTCA; *Sud1* Fw, GGTCGCAGCTGTTGGCCGAT; *Sud1* Rv, GTGGGACCAGCGCTGCAGTT; *Bip* Fw, GGCATTGATTTGGGCACCACGTAT; *Bip* Rv, TGTTCTCGGGATTGGTGGTCAACT; *Tub* Fw, ATCCCCAACAACGTGAAGAC; *Tub* Rv, GCCTGAACATAGCGGTGAAC.

Antibody Staining. Larvae were dissected in PBS and then fixed in 4% (vol/vol) formaldehyde (Sigma) for 40 min (imaginal discs) or 2 h (fat body) at room temperature, and samples were then washed in PT (PBS + 0.3% Triton X-100) for the imaginal discs or PBST (PBS + 0.1% Tween-20) for the fat bodies. Thereafter, samples were incubated for 2 h in PT + 5% (wt/vol) BSA (PBT) and then incubated with the primary antibody in PBT for 2 h at room temperature or overnight at 4 °C. Tissues were then washed three times for 20 min and incubated for another 2 h at room temperature with the secondary antibody diluted in PT + 5% (vol/vol) normal goat serum + 300 nM DAPI. After washing, imaginal discs were separated and mounted in 80% (vol/vol) glycerol.

The primary antibodies used were mouse anti-Engrailed (Developmental Studies Hybridoma Bank—DSHB 4D9; 1/100), rabbit anti-P-eIf2α (Cell Signaling #9721; 1/100), and rabbit anti-GFP (Molecular Probes #6455; 1/1,000). Secondary antibodies were donkey anti-rabbit Cy2 (Jackson #711–225-152), goat anti-rabbit Cy3 (Jackson #111–165-144), and donkey anti-mouse Cy3 (Jackson #715–165-150).

For phalloidin and DAPI stainings, larvae were dissected, fixed, and washed in PBST, after which they were incubated for 1 h at room temperature in 0.165 μM Alexa Fluor 488 phalloidin in PT or PBST containing 300 nM DAPI. After several washes, tissues or organs were sorted and mounted in 80% glycerol.

Lysotracker staining and TUNEL analysis were carried out as previously described (12, 13).

Wing Discs DTT Treatments. Larvae were dissected and incubated for 4 h in Schneider medium containing 5 mM DTT. Imaginal discs were then used for anti-GFP immunostainings.

Cell Culture. *Drosophila* Schneider's line $S2R^+$ cells were maintained at 28 °C in Schneider media (Sigma) and supplemented with 10% (vol/vol) FBS (Gibco), 50 U/mL penicillin, and 50 μg/mL streptomycin in 75-cm^2 T-flasks (Greiner).

dsRNA Synthesis and S2 Cell RNAi Treatment. A fragment of the *sud1* gene was amplified by PCR from cDNA using T7-tailed oligonucleotides as primers [primer sequence: *Drosophila* RNAi Screening Centre (www.flyrnai.org/DRSC-DRS.html) #15388]. dsRNA was synthetized using the T7 Megascript kit (Ambion). The bathing method was used to introduce dsRNAs into the cells as previously described (14). Cells were incubated with the dsRNA for 5 d. For stress granule assays, 0.25 mM sodium arsenite was added to the medium for 2 h before the samples were processed.

Stress granule detection. Stress granules (SGs) in *Drosophila* $S2R^+$ cells were visualized by FISH for polyadenylated RNA using oligodT-Cy3 (Sigma), as previously indicated (15). The granules were analyzed automatically with the BUHO MATLAB script as previously described (16).

β-Galactosidase assay. For X-Gal stainings, embryos were dechorionated and fixed with 0.5% glutaraldehyde for 20 min. Embryos were then washed with PBST and incubated at 37 °C with the β-galactosidase synthetic substrate X-gal.

Western Blots. Western blots were carried out by standard procedures using ECL plus (GE, RPN2232). The primary antibodies used were rabbit anti-P-eIf2α (Cell Signaling #9721; 1/1,000) and anti–α Tubulin (Developmental Studies Hybridoma Bank—DSHB;

http://dshb.biology.uiowa.edu; 12G10; 1/10,000). Secondary peroxidase–conjugated antibodies used were donkey anti-mouse (Jackson ImmunoResearch #715-035-150; 1/5,000) and donkey anti-rabbit (Jackson ImmunoResearch #111-035-144; 1/5,000).

Protein Synthesis Assay. Forty wing imaginal discs were dissected and incubated in a custom-made L-amino acid mixture [^{14}C(U)] containing alanine, arginine, glutamic acid, lysine, and serine (Perkin-Elmer) for 30 min. The supernatant was then removed, and tissues were washed in PBS and lysed in RIPA buffer. Trichloroacetic acid–insoluble radioactivity relative to total radioactivity in the lysates was evaluated in duplicate measurements.

Whole-Protein MS of Ribosomal Proteins. Ribosomal protein masses were analyzed by reversed phase ultra-performance liquid chromatography (RP-UPLC) and electrospray ionization time-of-flight mass spectrometry (ESI-TOF MS). The method used a Waters BEH C4 reversed phase column (2.1 × 50 mm, 1.7-μm particle size, 300-Å pore size). A flow rate of 0.3 mL/min was used with the column held at 40 °C using a Waters Acquity UPLC system connected directly to a Waters LCT ESI-TOF MS. The column was equilibrated with solvent A (0.1% formic acid in water). Five microliters of ribosomal protein sample was injected onto the column, and proteins were eluted using a stepped gradient from solvent A to solvent B (0.1% formic acid in acetonitrile). The following MS parameters were used: polarity, ES+; capillary voltage, 3,000 V; Sample cone voltage, 35 V; desolvation temperature, 250 °C; cone gas flow rate, 30 L/h; desolvation gas flow (N_2), 500 L/h. The mass spectra were acquired from 420 to 2,500 *m/z* using MassLynx 4.1 software (Waters), and protein spectra were deconvoluted using Maxent 1 with a range of 3–30 kDa (0.1-Da resolution). Masses were confirmed using manual component analysis. Sodium formate was used for instrument calibration, and leucine enkephalin was used as the lockspray compound allowing online mass correction.

LC-MS/MS Protein Analysis. LC-MS/MS analysis of the digested material was initially performed on an Agilent 6520 Q-TOF mass analyzer after separation on a 43-mm × 75-μm Zorbax 300SB-C18 5-μm chip column (Agilent) using a 23-min gradient of 5–40% solvent B (solvent A: 2% MeCN, 0.1% HCOOH; solvent B: 95% MeCN, 0.1% HCOOH). Further analysis of selected biological samples were carried out by nano-ultra performance liquid chromatography tandem MS (nano-UPLC-MS/MS) using a 75-μm inner diameter × 25-cm C18 nanoAcquity UPLC column (1.7-μm particle size; Waters) with a 45-min gradient of 2–40% solvent B (solvent A: 99.9% H_2O, 0.1% HCOOH; solvent B: 99.9% MeCN, 0.1% HCOOH). The Waters nanoAcquity UPLC system (final flow rate, 250 nl/min; ~7,000 psi) was coupled to a Q-TOF Premier tandem mass spectrometer (Waters) run in positive ion mode. MS analysis was performed in data-directed analysis (DDA) mode with MS to MS/MS switching at precursor ion counts greater than 10 with a return from MS/MS to MS survey after 1 s (MS/MS collision energy is dependent on precursor ion mass and charge state). All raw MS data were processed using either the MassHunter Qualitative Analysis version B.01.03 (Agilent) or PLGS version 2.3 (Waters) software with deisotoping and deconvolution (converting masses with multiple charge states to $m/z = 1$). The mass accuracy of the raw data were corrected using Glu-fibrinopeptide for the Waters QTOF and the background ion from dodecamethylcyclohexasiloxane at 445.12 Da for the Agilent QTOF. MS/MS spectra of the digested biological samples (Agilent, mgf files; Waters, pkl files) were searched against the UniProtKB/Swiss-Prot database (version 2010.08.13; 519,348 sequences) database using Mascot version 2.3.01 (Matrix Science) with the following parameters: peptide tolerance, 0.2 Da; $^{13}C = 1$; fragment tolerance, 0.1 Da; missed cleavages, 2; instrument type, ESI-Q-TOF-IMM; fixed modification, carbamidomethylation (C); and variable modifications, deamidation (Asp, Glu), oxidation (Met, Asn, Pro), and dioxidation (Pro). All database searches were performed on human or the corresponding species' entries. Assignments of hydroxylation on sites identified by Mascot were verified by manual inspection. MS/MS spectra were processed for documentation using the MassHunter Qualitative Analysis and MassLynx (v. 4.1) software for the Agilent and Waters data, respectively.

Protein Expression, Purification, and Coexpression Studies. Proteins were heterologously expressed using *Escherichia coli* BL21-DE3 cells and purified with Äkta FPLC systems. Expression was induced by isopropyl-β-D-thiogalactosidase (typically 0.5 mM, ~14 h at 18 °C) before harvest. GST-RPS23$_{44–143}$ was expressed either alone (control) or coexpressed together with His$_6$-Sudestada1, and then lysed (200 mM NaCl in 50 mM Tris, pH 7.5) by sonication and purified using immobilized glutathione agarose affinity, followed by in-solution trypsinolysis.

1. Bernal A, Kimbrell DA (2000) Drosophila Thor participates in host immune defense and connects a translational regulator with innate immunity. *Proc Natl Acad Sci USA* 97(11):6019–6024.
2. Shiga YT-MM, Hayashi S (1996) A nuclear GFP/β-galactosidase fusion protein as a marker for morphogenesis in living Drosophila. *Dev Growth Differ* 38(1):99–106.
3. Lavista-Llanos S, et al. (2002) Control of the hypoxic response in Drosophila melanogaster by the basic helix-loop-helix PAS protein similar. *Mol Cell Biol* 22(19): 6842–6853.
4. Ryoo HD, Domingos PM, Kang MJ, Steller H (2007) Unfolded protein response in a Drosophila model for retinal degeneration. *EMBO J* 26(1):242–252.
5. Pulipparacharuvil S, et al. (2005) Drosophila Vps16A is required for trafficking to lysosomes and biogenesis of pigment granules. *J Cell Sci* 118(Pt 16):3663–3673.
6. Arsham AM, Neufeld TP (2009) A genetic screen in Drosophila reveals novel cytoprotective functions of the autophagy-lysosome pathway. *PLoS ONE* 4(6):e6068.
7. Zhang Y, et al. (2003) Rheb is a direct target of the tuberous sclerosis tumour suppressor proteins. *Nat Cell Biol* 5(6):578–581.
8. Tapon N, Ito N, Dickson BJ, Treisman JE, Hariharan IK (2001) The Drosophila tuberous sclerosis complex gene homologs restrict cell growth and cell proliferation. *Cell* 105(3):345–355.
9. Oldham S, Montagne J, Radimerski T, Thomas G, Hafen E (2000) Genetic and biochemical characterization of dTOR, the Drosophila homolog of the target of rapamycin. *Genes Dev* 14(21):2689–2694.
10. Gao X, et al. (2002) Tsc tumour suppressor proteins antagonize amino-acid-TOR signalling. *Nat Cell Biol* 4(9):699–704.
11. Bateman JR, Lee AM, Wu CT (2006) Site-specific transformation of Drosophila via phiC31 integrase-mediated cassette exchange. *Genetics* 173(2):769–777.
12. Milán M, Campuzano S, García-Bellido A (1996) Cell cycling and patterned cell proliferation in the wing primordium of Drosophila. *Proc Natl Acad Sci USA* 93(2): 640–645.
13. Scott RC, Juhász G, Neufeld TP (2007) Direct induction of autophagy by Atg1 inhibits cell growth and induces apoptotic cell death. *Curr Biol* 17(1):1–11.
14. Clemens JC, et al. (2000) Use of double-stranded RNA interference in Drosophila cell lines to dissect signal transduction pathways. *Proc Natl Acad Sci USA* 97(12): 6499–6503.
15. Loschi M, Leishman CC, Berardone N, Boccaccio GL (2009) Dynein and kinesin regulate stress-granule and P-body dynamics. *J Cell Sci* 122(Pt 21):3973–3982.
16. Perez-Pepe M, et al. (2012) BUHO: A MATLAB script for the study of stress granules and processing bodies by high-throughput image analysis. *PLoS ONE* 7(12):e51495.

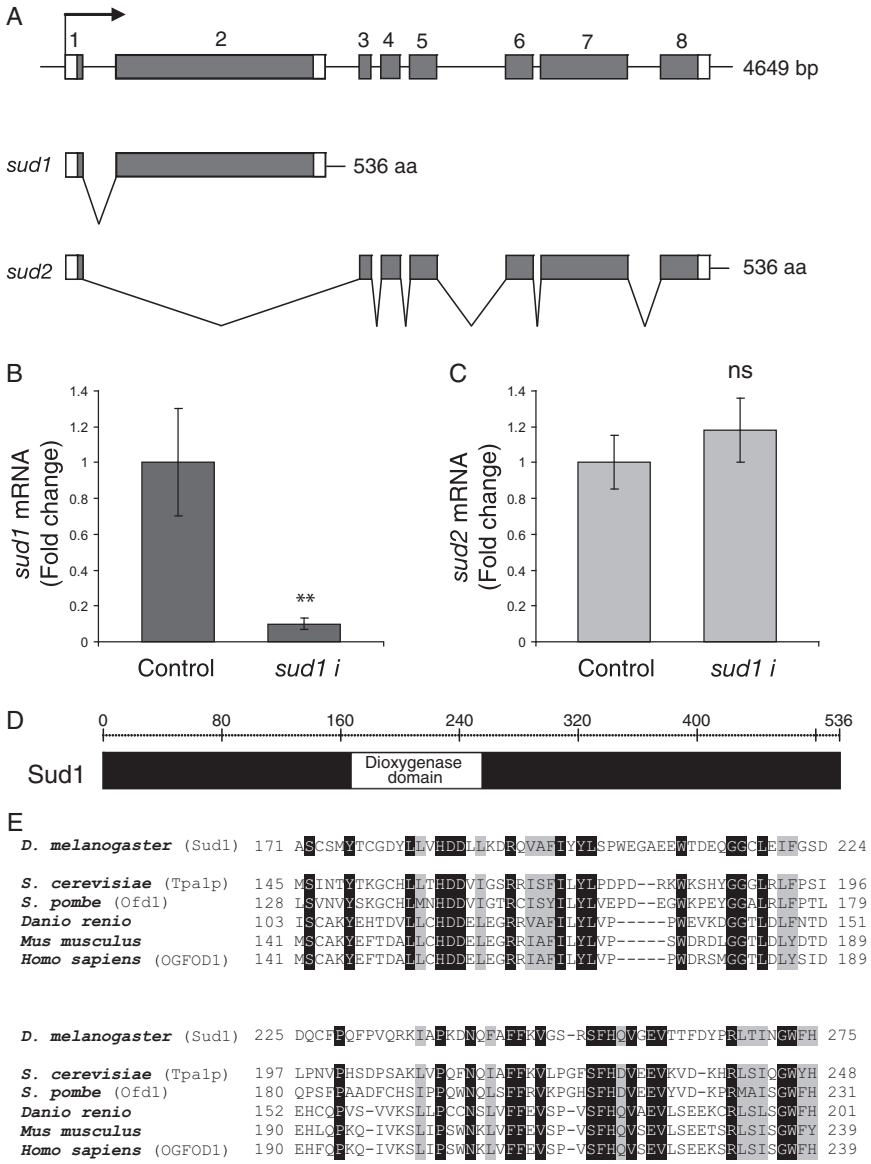

Fig. S1. The *sudestada* locus and RNAi-mediated silencing of *sud1* and *sud2* transcripts. (*A*) The locus *sudestada* (CG44254; www.flybase.org) encompasses eight exons and gives rise to two transcripts by alternative splicing, *sud1* and *sud2*, that have in common only exon 1. (*B* and *C*) *sudestada1* (*sud1*) and *sudestada2* (*sud2*) transcript levels were determined by qRT-PCR from total RNA extracted from first-instar larvae that express a *sud1* or a *white* (control) double-stranded RNA driven by *actin*-Gal4 in transgenic flies. Whereas *sud1* RNAi suppresses *sud1* transcript levels to less than 10% of control levels, the same RNAi does not affect *sud2* transcript levels. Error bars represent SD. (*D*) Sud1 protein includes a putative dioxygenase domain encoded by exon 2. (*E*) The *Drosophila* Sud1 dioxygenase domain is highly conserved in evolution. Identical amino acid residues are marked in black; amino acid residues displaying similarity between species are shown in gray.

Fig. S2. Sud1 silencing in the tracheal system and dorsal wing compartment. (*A–D*) Sud1 knockdown in the tracheal system does not affect HIF signaling in this tissue, as determined by the expression of an *ldh*-lacZ hypoxia inducible reporter in transgenic embryos, visualized by X-Gal staining. (*A*) Embryos expressing a *white* (control) double stranded RNA driven by *breathless*-Gal4 do not express the reporter in mild hypoxia (8% O_2). (*B*) The same embryos exposed to 5% O_2 display strong expression of the hypoxia-inducible reporter in tracheal cells (arrows). (*C*) Embryos exposed to mild hypoxia (8% O_2) and expressing a *fatiga* (*fga*) double stranded RNA under control of a *breathless*-Gal4 driver exhibit strong activation of the reporter in a pattern similar to that observed in *B* (arrows). (*D*) Embryos at 8%O_2 expressing *sud1* RNAi in the tracheal system do not activate the reporter, suggesting that Sud1 silencing does not activate HIF signaling. *sud1* (*E*) or *white* (control) (*F*) double-stranded RNAs were expressed in the wing disc dorsal compartment using a *ms1096*-Gal4 driver. Wings of flies expressing *sud1* but not a control RNAi are bended upward, indicating that the wing dorsal cell layer is smaller than the ventral layer. This wing phenotype implies that Sud1 silencing provokes growth impairment in this experimental setting.

A

GIVLEKYGVEAKQP (+15.99)NSAIR

Identified in MSS6793 1 x Oxidation (P)
Charge: 3, Exp. m/z: 675.388, Calc. m/z: 675.387

Max Intensity: 1.51 e+03

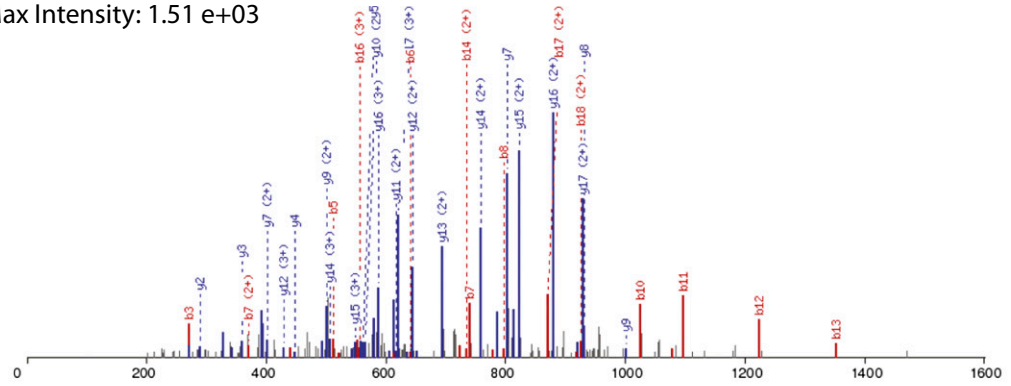

Key:	m/z out of range of spectrum	matched c-term ion	unmatched c-term ion	matched n-term ion	unmatched n-term ion

	G	I	V	L	E	K	V	G	V	E	A	K	Q	P	N	S	A	I	
	1	2	3	4	5	6	7	8	9	10	11	12	13	14	15	16	17	18	
a		143.12																	a
b		171.11	270.18	383.27	512.31	640.40	739.47	796.49	895.56	1024.60	1095.64	1223.74	1351.79	1464.84	1578.88	1665.92	1736.95	1850.04	b
b–15.99														1448.85	1562.89	1649.92	1720.96	1834.04	b–15.99
b (2+)						320.71	370.24	398.75	448.28	512.81	548.32	612.37	676.40	732.92	789.95	833.46	868.98	925.52	b (2+)
b–15.99 (2+)														724.93	781.95	825.46	860.98	917.53	b–15.99 (2+)
b (3+)												408.58	451.27	488.95	526.97	555.98	579.66	617.35	b (3+)
b–15.99 (3+)														483.62	521.63	550.65	574.32	612.02	b–15.99 (3+)
y		1967.13	1854.04	1754.98	1641.89	1512.85	1384.75	1285.69	1228.66	1129.60	1000.55	929.52	801.42	673.36	560.32	446.27	359.24	288.20	y
y–15.99		1951.13	1838.05	1738.98	1625.90	1496.85	1368.76	1269.69	1212.67	1113.60	984.56	913.52	785.43	657.37					y–15.99
y (2+)		984.07	927.53	877.99	821.45	756.93	692.88	643.35	614.84	565.30	500.78	465.26	401.21	337.19	280.66	223.64	180.12	144.61	y (2+)
y–15.99 (2+)		976.07	919.53	869.99	813.45	748.93	684.88	635.35	606.84	557.30	492.78	457.26	393.22	329.19					y–15.99 (2+)
y (3+)		656.38	618.69	585.66	547.97	504.95	462.26	429.23	410.23	377.20	334.19	310.51							y (3+)
y–15.99 (3+)		651.05	613.35	580.33	542.64	499.62	456.92	423.90	404.89	371.87	328.86	305.18							y–15.99 (3+)
	G	I	V	L	E	K	V	G	V	E	A	K	Q	P	N	S	A	I	
	19	18	17	16	15	14	13	12	11	10	9	8	7	6	5	4	3	2	

	R	
	19	
a		a
b		b
b–15.99		b–15.99
b (2+)		b (2+)
b–15.99 (2+)		b–15.99 (2+)
b (3+)		b (3+)
b–15.99 (3+)		b–15.99 (3+)
y	175.12	y
y–15.99		y–15.99
y (2+)	88.06	y (2+)
y–15.99 (2+)		y–15.99 (2+)
y (3+)		y (3+)
y–15.99 (3+)		y–15.99 (3+)
	R	
	1	

Fig. S3. (Continued)

B
GIVLEKYGVEAKQP (+15.99)NSAIR

Identified in MSS6793 1 x Oxidation (P)
Charge: 3, Exp. m/z: 675.389, Calc. m/z: 675.387

Max Intensity: 1.49 e+03

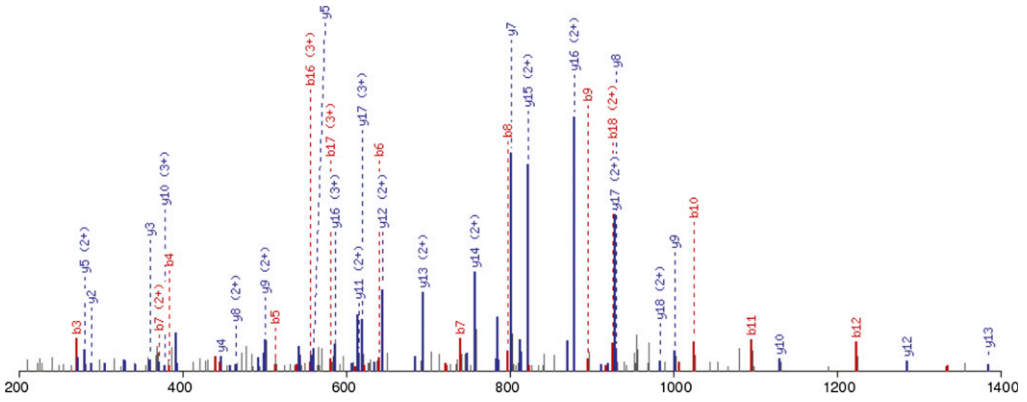

Key: m/z out of range of spectrum | matched c-term ion | unmatched c-term ion | matched n-term ion | unmatched n-term ion

	G	I	V	L	E	K	V	G	V	E	A	K	Q	P	N	S	A	I	
	1	2	3	4	5	6	7	8	9	10	11	12	13	14	15	16	17	18	
a		143.12																	a
b		171.11	270.18	383.27	512.31	640.40	739.47	796.49	895.56	1024.60	1095.64	1223.74	1351.79	1464.84	1578.88	1665.92	1736.95	1850.04	b
b--15.99														1448.85	1562.89	1649.92	1720.96	1834.04	b--15.99
b (2+)						320.71	370.24	398.75	448.28	512.81	548.32	612.37	676.40	732.92	789.95	833.46	868.98	925.52	b (2+)
b--15.99 (2+)														724.93	781.95	825.46	860.98	917.53	b--15.99 (2+)
b (3+)												408.58	451.27	488.95	526.97	555.98	579.66	617.35	b (3+)
b--15.99 (3+)														483.62	521.63	550.65	574.32	612.02	b--15.99 (3+)
y		1967.13	1854.04	1754.98	1641.89	1512.85	1384.75	1285.69	1228.66	1129.60	1000.55	929.52	801.42	673.36	560.32	446.27	359.24	288.20	y
y--15.99		1951.13	1838.05	1738.98	1625.90	1496.85	1368.76	1269.69	1212.67	1113.60	984.56	913.52	785.43	657.37					y--15.99
y (2+)		984.07	927.53	877.99	821.45	756.93	692.88	643.35	614.84	565.30	500.78	465.26	401.21	337.19	280.66	223.64	180.12	144.61	y (2+)
y--15.99 (2+)		976.07	919.53	869.99	813.45	748.93	684.88	635.35	606.84	557.30	492.78	457.26	393.22	329.19					y--15.99 (2+)
y (3+)		656.38	618.69	585.66	547.97	504.95	462.26	429.23	410.23	377.20	334.19	310.51							y (3+)
y--15.99 (3+)		651.05	613.35	580.33	542.64	499.62	456.92	423.90	404.89	371.87	328.86	305.18							y--15.99 (3+)
	G	I	V	L	E	K	V	G	V	E	A	K	Q	P	N	S	A	I	
	19	18	17	16	15	14	13	12	11	10	9	8	7	6	5	4	3	2	

	R	
	19	
a		a
b		b
b--15.99		b--15.99
b (2+)		b (2+)
b--15.99 (2+)		b--15.99 (2+)
b (3+)		b (3+)
b--15.99 (3+)		b--15.99 (3+)
y	175.12	y
y--15.99		y--15.99
y (2+)	88.06	y (2+)
y--15.99 (2+)		y--15.99 (2+)
y (3+)		y (3+)
y--15.99 (3+)		y--15.99 (3+)
	R	
	1	

Fig. S3. (Continued)

C

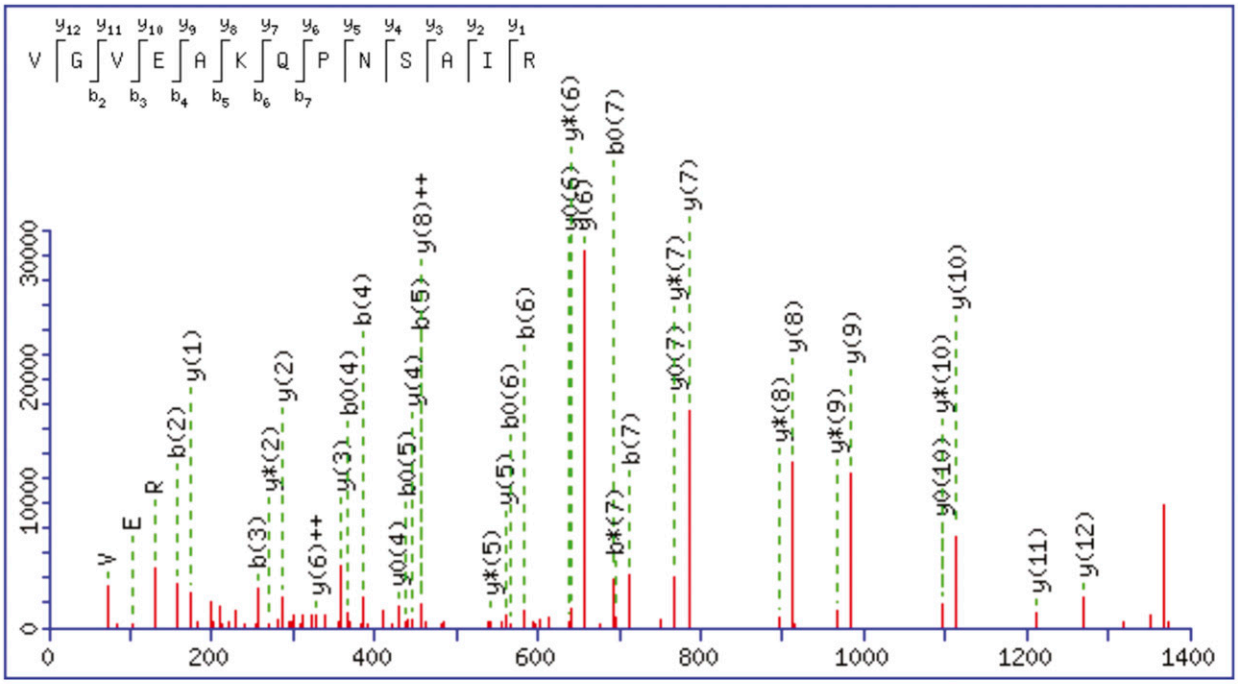

D

#	Immon.	b	b^{++}	b*	b^{*++}	b^0	b^{0++}	Seq.	y	y^{++}	y*	y^{*++}	y^0	y^{0++}	#
1	**72.0808**	100.0757	50.5415					V							13
2	30.0338	**157.0972**	79.0522					G	**1269.6910**	635.3491	1252.6644	626.8359	1251.6804	626.3438	12
3	**72.0808**	**256.1656**	128.5864					V	**1212.6695**	606.8384	1195.6430	598.3251	1194.6589	597.8331	11
4	**102.0550**	**385.2082**	193.1077			**367.1976**	184.1024	E	**1113.6011**	557.3042	**1096.5745**	548.7909	**1095.5905**	548.2989	10
5	44.0495	**456.2453**	228.6263			**438.2347**	219.6210	A	**984.5585**	492.7829	**967.5320**	484.2696	966.5479	483.7776	9
6	101.1073	**584.3402**	292.6738	567.3137	284.1605	**566.3297**	283.6685	K	**913.5214**	**457.2643**	**896.4948**	448.7511	895.5108	448.2591	8
7	101.0709	**712.3988**	356.7030	**695.3723**	348.1898	**694.3883**	347.6978	Q	**785.4264**	393.2169	**768.3999**	384.7036	**767.4159**	384.2116	7
8	70.0651	809.4516	405.2294	792.4250	396.7162	791.4410	396.2241	P	**657.3678**	**329.1876**	**640.3413**	320.6743	**639.3573**	320.1823	6
9	87.0553	923.4945	462.2509	906.4680	453.7376	905.4839	453.2456	N	**560.3151**	280.6612	**543.2885**	272.1479	542.3045	271.6559	5
10	60.0444	1010.5265	505.7669	993.5000	497.2536	992.5160	496.7616	S	**446.2722**	223.6397	429.2456	215.1264	**428.2616**	214.6344	4
11	44.0495	1081.5636	541.2855	1064.5371	532.7722	1063.5531	532.2802	A	**359.2401**	180.1237	342.2136	171.6104			3
12	86.0964	1194.6477	597.8275	1177.6212	589.3142	1176.6371	588.8222	I	**288.2030**	144.6051	**271.1765**	136.0919			2
13	**129.1135**							R	**175.1190**	88.0631	158.0924	79.5498			1

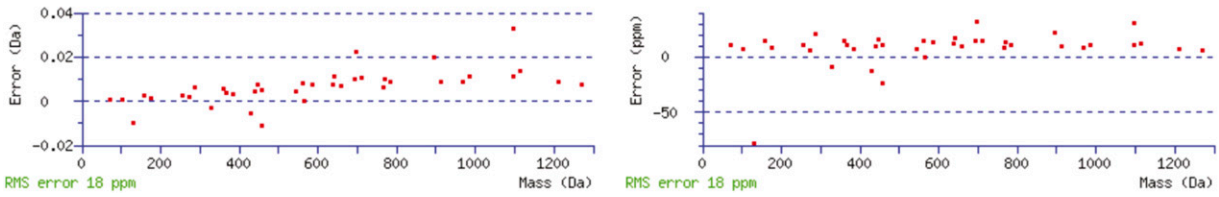

Fig. S3. (Continued)

E

#	Immon.	b	b^{++}	b*	b^{*++}	b^{0}	b^{0++}	Seq.	y	y^{++}	y*	y^{*++}	y^{0}	y^{0++}	#
1	**72.0808**	100.0757	50.5415					V							13
2	30.0338	**157.0972**	79.0522					G	**1285.6859**	**643.3466**	1268.6593	634.8333	1267.6753	634.3413	12
3	**72.0808**	**256.1656**	128.5864					V	**1228.6644**	614.8359	1211.6379	606.3226	1210.6539	605.8306	11
4	**102.0550**	**385.2082**	193.1077			**367.1976**	184.1024	E	**1129.5960**	**565.3016**	1112.5695	**556.7884**	**1111.5854**	**556.2964**	10
5	44.0495	**456.2453**	228.6263			**438.2347**	219.6210	A	**1000.5534**	500.7803	**983.5269**	492.2671	982.5429	491.7751	9
6	**101.1073**	**584.3402**	292.6738	567.3137	284.1605	566.3297	283.6685	K	**929.5163**	465.2618	**912.4898**	456.7485	911.5057	**456.2565**	8
7	**101.0709**	**712.3988**	356.7030	**695.3723**	348.1898	694.3883	347.6978	Q	**801.4213**	401.2143	**784.3948**	392.7010	**783.4108**	392.2090	7
8	86.0600	825.4465	413.2269	808.4199	404.7136	807.4359	404.2216	P	**673.3628**	337.1850	**656.3362**	328.6717	**655.3522**	**328.1797**	6
9	87.0553	939.4894	470.2483	922.4629	461.7351	921.4789	461.2431	N	**560.3151**	280.6612	**543.2885**	272.1479	542.3045	271.6559	5
10	60.0444	1026.5215	513.7644	1009.4949	505.2511	1008.5109	504.7591	S	**446.2722**	223.6397	**429.2456**	215.1264	**428.2616**	214.6344	4
11	44.0495	1097.5586	549.2829	1080.5320	540.7696	1079.5480	540.2776	A	**359.2401**	180.1237	342.2136	171.6104			3
12	86.0964	1210.6426	605.8250	1193.6161	597.3117	1192.6321	596.8197	I	**288.2030**	144.6051	**271.1765**	136.0919			2
13	**129.1135**							R	**175.1190**	88.0631	158.0924	79.5498			1

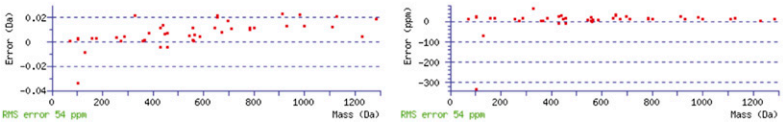

Fig. S3. Tandem MS assignment of Arg-C peptide species (*m/z* 675.388) as hydroxylated [M+3H]3+ RPS23 peptide amino acids 49–67. (*A* and *B*) Database search of the *m/z* 675.388 species detected by LC-MS/MS in the retention time range of 37.5 min assigns the peptide species with statistical significance as being GIVLEKVGVEAKQPNSAIR from RPS23, carrying a 16-Da mass increment (hydroxylation) on either Gln-61 or Pro-62. The fragment ion mass corresponding to the y6 ion (673.36 Da), which would formally assign Pro-62 as the site of modification, is not recorded by the ion trap mass analyzer. However, coverage of the remaining y-ions, ranging from the y2 ion to the y11 ion indicates a 16-Da mass shift on the adjacent y7 fragment ion, localizing the modification to Gln-61 or Pro-62. Formal (unambiguous) assignment of Pro-62 hydroxylation on a related peptide is provided in Fig. 3*E*. MS/MS assignment of *m/z* 670.057 was not possible owing to the low abundance of the precursor ion. However, the exact mass and retention time of the *m/z* 670.057 species are consistent with the unmodified peptide GIVLEKVGVEAKQPNSAIR (which is identical in human rpS23) and formally assigned in a companion article. (*C*) LC-MS/MS analysis of trypsinized GST-RPS23. In the absence of Sudestada1, RPS23 Pro-62 was unmodified (control experiment for data reported in Fig. 3*E*). The b and y fragment ions are indicated (peptide precursor ion: M_r 1,367.691848 Da; calculated 1,367.7521 Da). (*D*) Tables of observed MS/MS fragment ions of trypsinized GST-RPS23 depicted in *C*. Control experiment of RPS23 55-VGVEAKQPNSAIR-67 lacking modification at Pro-62. (*E*) Tables of observed MS/MS fragment ions of trypsinized GST-RPS23 depicted in Fig. 3*E*. RPS23 55-VGVEAKQPNSAIR-67 monohydroxylated (+16 Da) at Pro-62 after coexpression with His6-Sudestada1. The table lists the b, y, and immonium fragment ions.

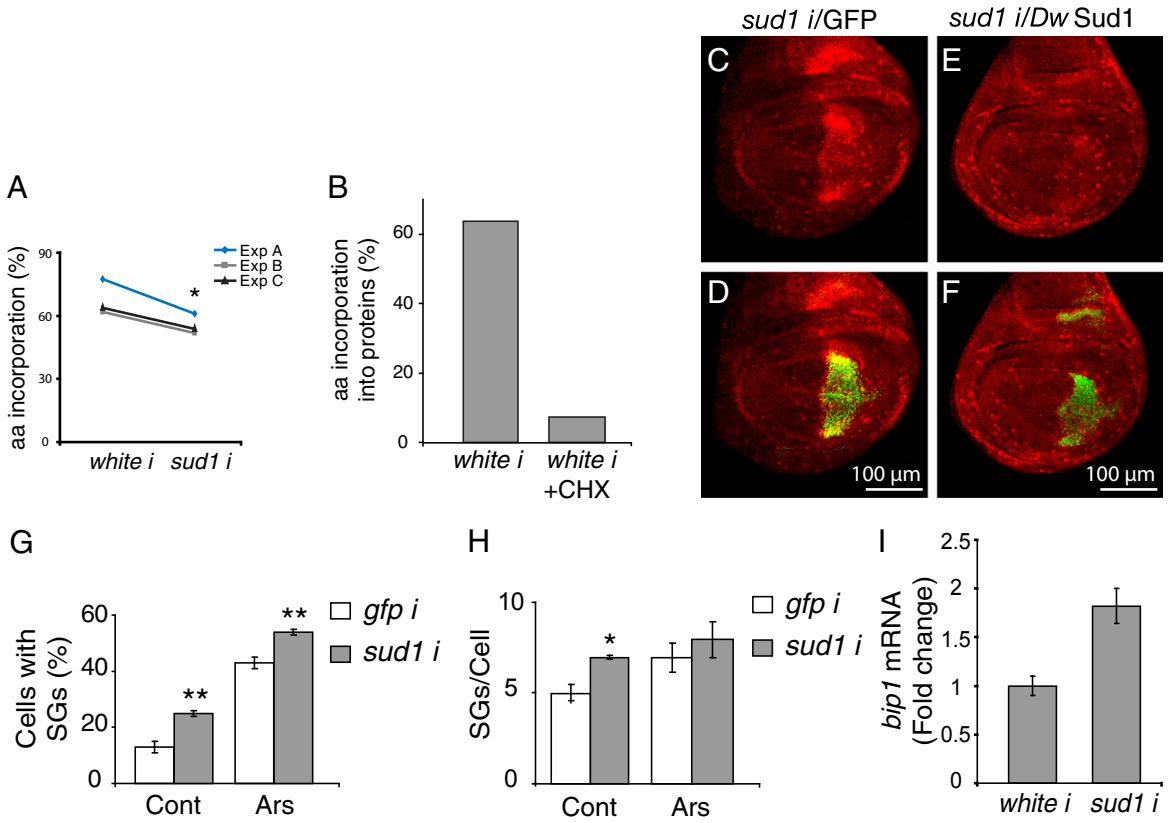

Fig. S4. Sud1 silencing inhibits protein synthesis, promotes stress granule formation, and triggers the unfolded protein response. (*A*) Sud1 silencing inhibits protein synthesis. Third-instar larvae wing imaginal discs were incubated with a mixture of [^{14}C]-labeled amino acids, and disc extracts were subjected to trichloroacetic acid (TCA) precipitation; the proportion of TCA-precipitated radioactivity in relation to total radioactivity incorporated into the discs in three independent experiments is shown ($n = 40$ discs). Data were analyzed with randomized blocks ANOVA. Paired measurements (including the two genotypes; $^{*}P < 0.05$). (B) Ex vivo incorporation of [^{14}C]-labeled amino acids into proteins of wing discs is strongly suppressed in a negative control experiment in which cycloheximide has been added to the incubation medium. (*C* and *D*) Wing discs accumulate P-eIF2a at the posterior compartment after expression of *sud1* RNAi. This accumulation is suppressed by concomitant expression of a *sud1 Drosophila willistoni* transgene (*E* and *F*), indicating that augmented phosphorylation of eIF2a is indeed due to Sud1 silencing. Green, anti-Engrailed staining. Quantification of the cells exhibiting SGs (*G*), as well as of the number of SGs per cell (*H*), was carried out automatically using the BUHO algorithm (*Materials and Methods*). Error bars represent SD. Two-way ANOVA with Bonferroni post hoc test ($^{*}P < 0.01$ and $^{**}P < 0.001$). (*I*) The Xbp-1 target *bip1* is induced after *actin*-Gal4 driven expression of *sud1* but not of *white* RNAi in first-instar larvae, as determined by qRT-PCR; error bars represent SD.

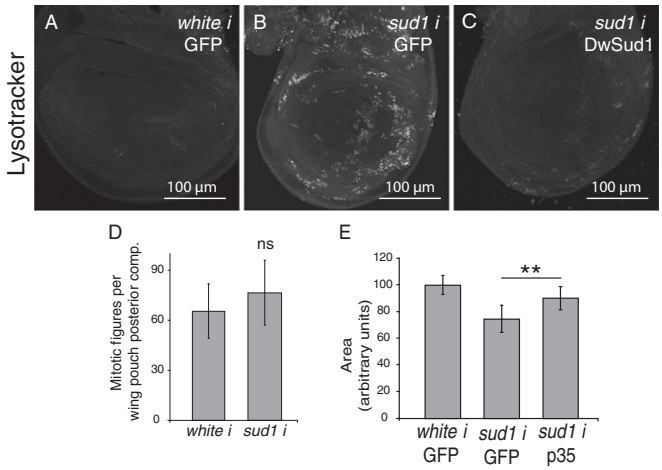

Fig. S5. After Sud1 silencing, autophagy and apoptosis are induced, but cell proliferation is unaffected. Lysotracker-positive staining in the posterior compartment of wing discs that express *sud1* RNAi (*B*) but not a control *white* RNAi (*A*) indicates that Sud1 silencing triggers autophagy. The Lysotracker-positive signal is suppressed after concomitant expression of a *Drosophila willistoni sud1* transgene (*C*). (*D*) *sud1* RNAi expression in the wing disc posterior compartment does not modify the number of cells that enter mitosis, as assessed by anti–phospho-Histone3 (PH3) immunofluorescence. The number of PH3-positive cells was analyzed in discs expressing *sud1* RNAi in comparison with control discs that express a *white* double stranded RNA. $n \geq 10$ imaginal discs. Error bars represent SD. ns, nonsignificant difference (Student *t* test). (*E*) Reduction of the area of the wing posterior compartment is partially suppressed by expression of the caspase inhibitor p35. $n \geq 30$ wings in three independent experiments. Error bars represent SD. One-way ANOVA with Tukey post hoc test (**$P < 0.01$).

Table S1. Loss of function screen for *Drosophila* dioxygenases required for wing normal growth

Gene	RNAi Line (VDRC number)	Intensity of growth phenotype	References
CG31543 (Fatiga)	KK103382	++	1
CG8421	KK101484	+	
CG44254	GD3402	+++	
CG31014	KK101152	–	
CG18749	GD15364	–	
CG9698	KK100678	–	
CG31022	GD2464	–	
CG9720	KK100523	–	
CG9726	KK101283	–	
CG31016	GD21280	–	
CG9728	KK102038	–	
CG18233	KK101594	–	
CG1546	KK107425	–	
CG32199	GD21601/ GD21600	–	
CG31524	KK100877	–	
CG32201	GD47008	–	
CG15864	KK105061	+	
CG18231	KK101201	–	
CG11828	KK101020	–	
CG18234	GD19187	–	
CG6199	GD45486/ GD45484	–	
CG7200	GD27913	–	
CG10133	GD18014/ KK108848	–	
CG2982	KK107819	+	
CG5640 (dUTX)	GD37664/ GD37663/ KK105986	+	2–4
CG9088 (LID)	KK103830/ GD42204	++	5, 6
CG33182 (dKdm4B)	GD46444	–	7
CG15835 (dKdm4A)	KK107868	+	8, 9
CG3654	GD21700	–	
CG11033 (dKdm2)	GD31402	–	10
CG33250	GD46450/ GD46452	–	
CG4036	GD26370	–	
CG6144	GD41847	–	
CG14130	GD31911	–	
CG14688	GD39840	–	
CG4335	KK105611	–	
CG10814	KK108425	–	
CG5321	GD22061	–	
CG14630	KK101204	+++	
CG33099	KK104229	–	
CG5346	KK101879	–	
CG33093	GD48795/ GD48796	–	

An RNAi-based screen was carried out to define which *Drosophila* dioxygenases are required for normal wing growth. Double-stranded RNAs (second column) against each of the predicted 2OG-dependent dioxygenases encoded in the *Drosophila* genome (first column) were expressed in transgenic lines under control of an *ms1096*-Gal4 driver, which induces expression exclusively at the disc dorsal compartment. Inhibition of growth of this compartment leads to development of wings that are curved upward. Depending on the intensity of the wing curvature, the phenotypes were classified as strong (+++), intermediate (++), or weak (+) (third column). Nine of the 42 presumptive dioxygenases scored as positives in the screen. The names of the genes that have been analyzed are quoted in parentheses, and the corresponding references are in the fourth column of the table.

1. Centanin L, Ratcliffe PJ, Wappner P (2005) Reversion of lethality and growth defects in Fatiga oxygen-sensor mutant flies by loss of hypoxia-inducible factor-alpha/Sima. *EMBO Rep* 6(11):1070–1075.
2. Tie F, Banerjee R, Conrad PA, Scacheri PC, Harte PJ (2012) Histone demethylase UTX and chromatin remodeler BRM bind directly to CBP and modulate acetylation of histone H3 lysine 27. *Mol Cell Biol* 32(12):2323–2334.
3. Herz HM, et al. (2010) The H3K27me3 demethylase dUTX is a suppressor of Notch- and Rb-dependent tumors in Drosophila. *Mol Cell Biol* 30(10):2485–2497.
4. Smith ER, et al. (2008) Drosophila UTX is a histone H3 Lys27 demethylase that colocalizes with the elongating form of RNA polymerase II. *Mol Cell Biol* 28(3):1041–1046.
5. Secombe J, Li L, Carlos L, Eisenman RN (2007) The Trithorax group protein Lid is a trimethyl histone H3K4 demethylase required for dMyc-induced cell growth. *Genes Dev* 21(5): 537–551.
6. Lee N, et al. (2007) The trithorax-group protein Lid is a histone H3 trimethyl-Lys4 demethylase. *Nat Struct Mol Biol* 14(4):341–343.
7. Palomera-Sanchez Z, Bucio-Mendez A, Valadez-Graham V, Reynaud E, Zurita M (2010) Drosophila p53 is required to increase the levels of the dKDM4B demethylase after UV-induced DNA damage to demethylate histone H3 lysine 9. *J Biol Chem* 285(41):31370–31379.
8. Lin CH, et al. (2008) Heterochromatin protein 1a stimulates histone H3 lysine 36 demethylation by the Drosophila KDM4A demethylase. *Mol Cell* 32(5):696–706.
9. Lorbeck MT, et al. (2010) The histone demethylase Dmel\Kdm4A controls genes required for life span and male-specific sex determination in Drosophila. *Gene* 450(1-2):8–17.
10. Lagarou A, et al. (2008) dKDM2 couples histone H2A ubiquitylation to histone H3 demethylation during Polycomb group silencing. *Genes Dev* 22(20):2799–2810.

Table S2. Reduction of function of the TOR pathway partially suppresses growth inhibition provoked by Sudestada1 silencing

Allele	Nuclear area (% of control)		Nuclear area reduction (%)(*white* RNAi − *sud1* RNAi)
	white RNAi	*sud1* RNAi	
yw	100 ± 18.8	61 ± 10.2	39
tor^{2L1}	97.2 ± 14.5	86.4 ± 13.6**	11.2
tsc^{Q87X}	98.9 ± 12.5	61.3 ± 20.4	38
$S6K^{L1}$	94.9 ± 17.3	78.6 ± 17.3**	17.2
$rheb^{P\Delta1}$	93.9 ± 11.3	66.7 ± 16	29
$rheb^{P\Delta2}$	94 ± 12.4	68.2 ± 16.8	27.4
4E-BP ($thor^2$)	91 ± 10.8	48.3 ± 6.9*	46.9

sud1 RNAi was expressed under control of a *ppl*-Gal4 driver, and the area of nuclei of fat body cells was measured in third-instar larvae that were heterozygous for the indicated loss of function alleles of genes of the TOR pathway. Note that growth inhibition provoked by *sud1* RNAi expression is alleviated in TOR^{2L1} and $S6K^{L1}$ heterozygous larvae, and conversely, it is enhanced in 4E-BP($thor^2$) heterozygous individuals. $n \geq 300$ nuclei in three independent experiments. Error bars represent SD. Two-way ANOVA with Tukey post hoc test (*$P < 0.05$ and **$P < 0.001$). In the case of 4E-BP, the data were transformed to $\log_{10}$.